ICAS 2020 SHANG HAI
International Council of the Aeronautical Sciences
32nd Congress of the International Council of the Aeronautical Sciences
September 6-10, 2021
Pudong Shangri-La, Shanghai, China

AERODYNAMIC ANALYSIS OF A HIGH SPEED TEST RIG FOR USE IN ENGINE TEST FACILITIES

Faezeh Rasimarzabadi[1], Martin Neuteboom[1], Catherine Clark[2], & Hans Martensson[3]

[1]National Research Council of Canada, Gas Turbine Laboratory, Ottawa, Canada

[2]National Research Council of Canada, Aerodynamic Laboratory, Ottawa, Canada

[3]GKN Aerospace Engine Systems, Trollhattan, Sweden

Abstract

A boundary layer ingestion (BLI) test rig has been developed by National Research Council of Canada in Ottawa for studying a sub-scale BLI propulsion technology that has the potential to reduce aircraft fuel consumption by improving the propulsion efficiency of aircraft engines. This paper provides details of the aerodynamic design and analysis of the related test rig. This BLI rig is unique compared to most known projects in that it is capable of achieving representative cruise flight altitudes and Mach numbers while most other known studies have been performed at sea level and lower speeds. The results include CFD simulation of applying an ejector to get high subsonic flow at the tunnel test section, as the first option, then modifying the existing high altitude test rig at different parts, as a better option for a BLI test rig.

Keywords: Aerodynamic, Propulsion, Boundary layer ingestion (BLI), Computational Fluid Dynamics (CFD)

1. Introduction

Boundary layer ingestion (BLI) is a concept where the engine ingests the boundary layer developed over the length of the aircraft and is seen as a potential technique to improve the overall aircraft propulsive efficiency and reduce fuel consumption. Aerodynamic and engine testing have traditionally been done in isolation, but for these future aircraft designs, there would be a need to have an integrated technology demonstrator that combine the testing of the intake with BLI and the engine.

A constant effort is being made by aircraft engine manufacturers to reduce fuel burn through technological advancements. Next generation aircraft – from business jets to wide-body aircraft – are predicted to have distributed propulsion systems that use future propulsion concepts (e.g. hybrid/electric) and blended wing bodies. These designs use engines embedded in the fuselage with boundary layer ingestion. There are several architectures which allow the ingestion of the boundary layer [1- 5]. The technology operates through ingesting slow moving boundary layer flow into the engines in order to produce the requisite thrust. The benefits are achieved by reducing drag, decreasing the amount of required thrust, and improving overall propulsive efficiency. A list of analysis was compiled showing between 3 and 10% benefit in applying BLI [6]. The wide range in results reported on BLI potential performance was one reason that NRC prompted to undertake a test campaign to get some validation data.

2. Test Rig Design Using Ejector

Initially for the test rig configuration, it was assumed that the use of existing ejectors were required to reach the required Mach number at the test section. Ejector systems have the main advantage of not containing any moving parts and have long been attractive in a wide range of applications such as refrigeration, vacuum pumps, cooling, thrust augmentation, power generation, and chemical

processing [7- 11]. The application of ejectors for wind tunnel has rarely been studied in the past [12].

In this concept, the primary flow is supplied by high pressure air and accelerated through up to four convergent-divergent nozzles that were designed and tested in the past at the NRC [13], Figure 1. A high velocity jet is produced in choked condition at the nozzle exit. This entrains the secondary flow which is ambient air at room temperature and pressure. The two air flows then combine by the end of the mixing chamber.

The performance of the ejector was calculated using one-dimensional mass, momentum and energy conservation equations by considering a few assumptions and applying some iterative means to solve a set of simultaneous equations [14]. Figure 2 shows the preliminary dimensions of the test rig obtained through the design procedure [15]. In this design, the total length of the test rig was calculated to be about 18m.

The one-dimensional method provides a simple and reasonably accurate estimate, but with limited geometrical information. The CFD simulation is used as a design tool to improve the operation of ejectors by detailed analysis of the flow features within the ejector.

Figure 1 – A picture of the ejector nozzles

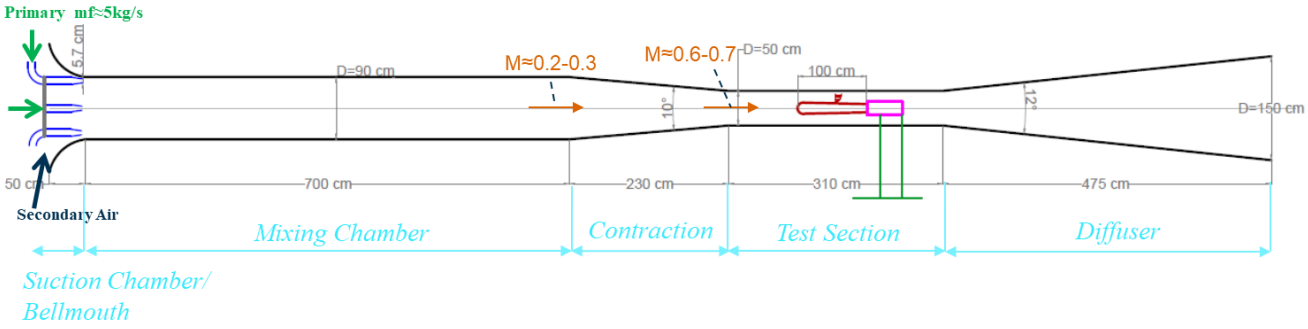

Figure 2 – Schematic of the possible test rig configuration using ejector system

2.1 Numerical Analysis

The flow field was studied using ANSYS FLUENT V2019. Figure 3 shows an example of Mach number contours of the 2-D model applying two nozzles at a total pressure of 340 kPa and a total mass flow rate of 5 kg/s. The CFD model was steady and density based. The solution method was implicit with flux type of Roe-FDS. The k-epsilon turbulence model with standard wall functions was selected. The entire solution domain was discretized using an unstructured grid. The results confirm that a Mach number of about 0.7 is achievable at the test section.

Figure 4 shows the effect of nozzle total pressure on velocity profiles at mid test section and Figure 5 shows the ejector mass flow ratio, which is the ratio of the secondary mass flow to the primary mass flow, ω. By further analysis of the operating conditions such as nozzle pressure and geometrical factors such as the length of the mixing chamber or the number of nozzles, the optimum ejector

performance could be achieved.

However, due to space limitation for an 18m-length ejector rig, and to reduce the cost of fabrication, it was found that an existing compressor rig [16, 17] could be adapted for a BLI test rig by making some changes. The advantage was the possibility to test at high altitudes.

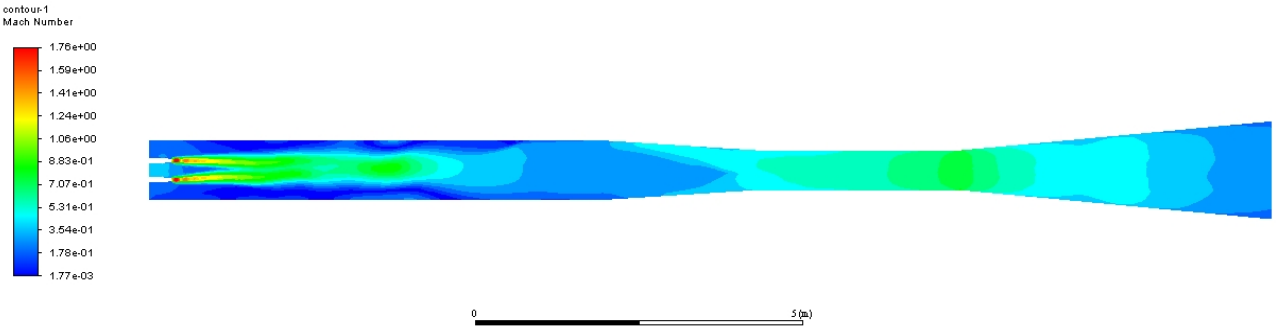

Figure 3 – Mach number contour, two-nozzle, P_0=340 kPa

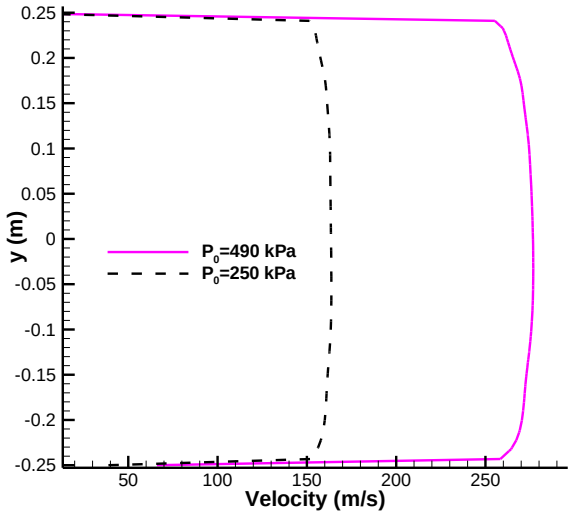

Figure 4 – Nozzle pressure effect on velocity profile at the middle of the test section

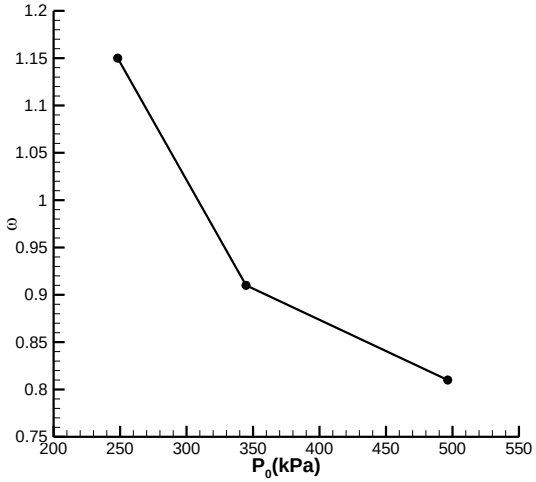

Figure 5 – Effect of P_0 of nozzle on ejector mass flow ratio

3. Altitude Compressor Rig

The plenum used to create altitude pressure is shown in Figure 6. The plenum consists of an inlet bell mouth, a series of flanged pipe sections in which the compressor is mounted, a gate valve to throttle the inlet flow, perforated plates to further reduce pressure and turbulence, and a suction pipe which is connected to an exhauster that creates the flow through the plenum. Suction is provided

through the suction pipe to create a mass flow through the plenum. The gate valve is then progressively closed to create the desired pressures. By varying the amount of suction pressure and the gate valve position, different flow rates and plenum pressures can be achieved. The test rig is capable of providing altitude up to 38000 ft and flight speeds of Mach 0.74.

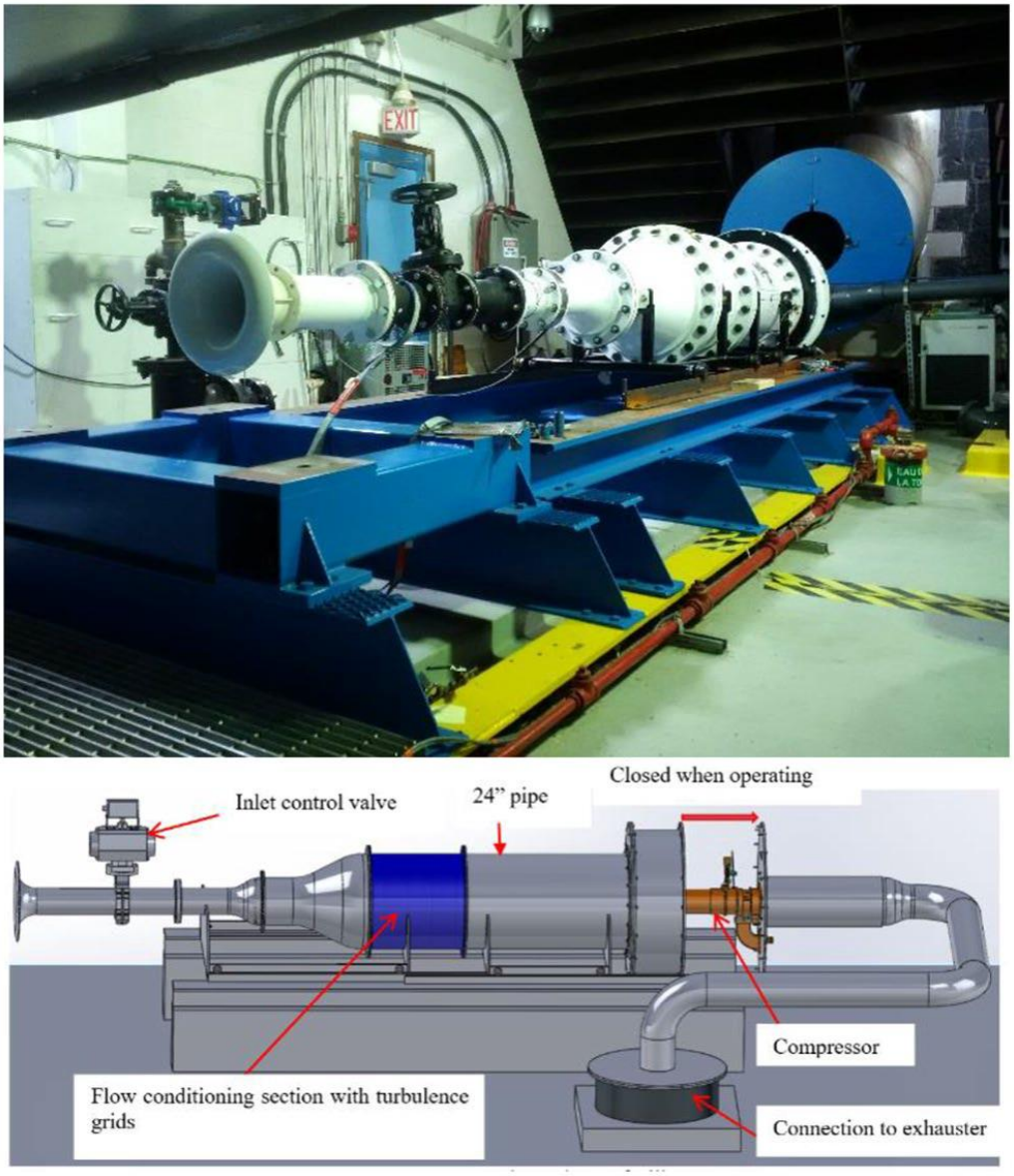

Figure 6 – Altitude compressor rig

3.1 Plenum Modifications

Since the altitude plenum needs to provide the air flow as an internal flow to the propulsion system, the test section diameter should be the same as the scaled propulsion system diameter which is 180 mm. A contraction was designed to connect the 61 cm (24 inch) pipe to the test section, Figure 7. At the downstream, the test section is connected to the U-shape exhaust tube.

A boundary layer body representing the aircraft geometry with diameter of 90 mm is mounted within the plenum to create a natural boundary layer due to skin friction.

After some CFD analysis, it was found that the boundary layer of the test section wall affects the velocity profile at the inlet of the propulsion system. Therefore, the effect of test section walls was required to be removed. In order to resolve the problem, a bypass nacelle was designed as shown in Figure 8. Based on the estimated maximum boundary layer of the test section walls, the diameter of the new test section was estimated as 250 mm, Figure 8.

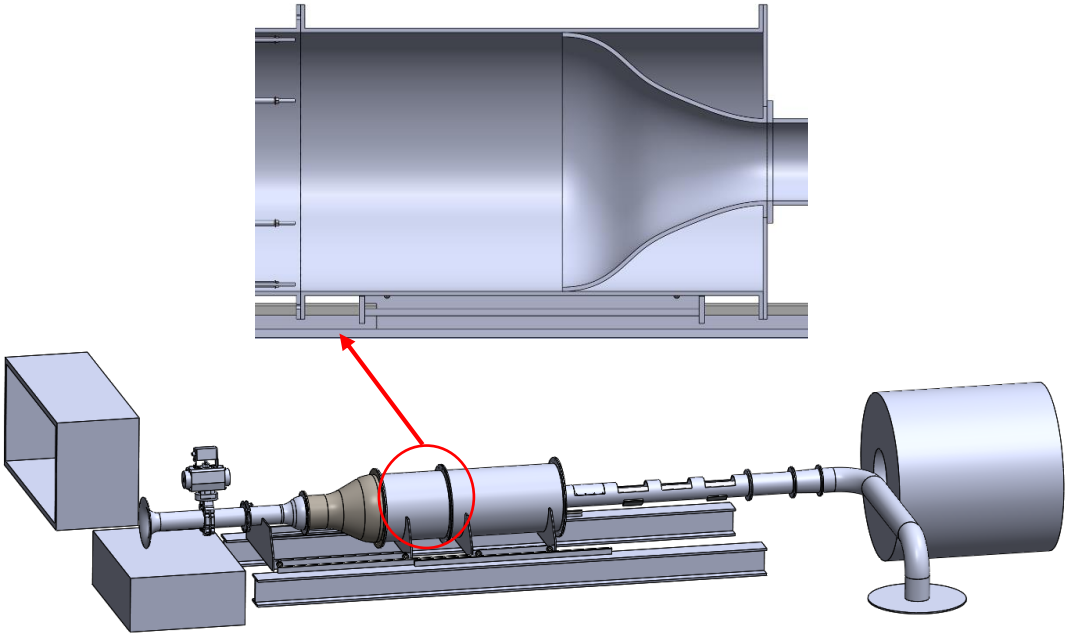

Figure 7 – Modified concept for the contraction part

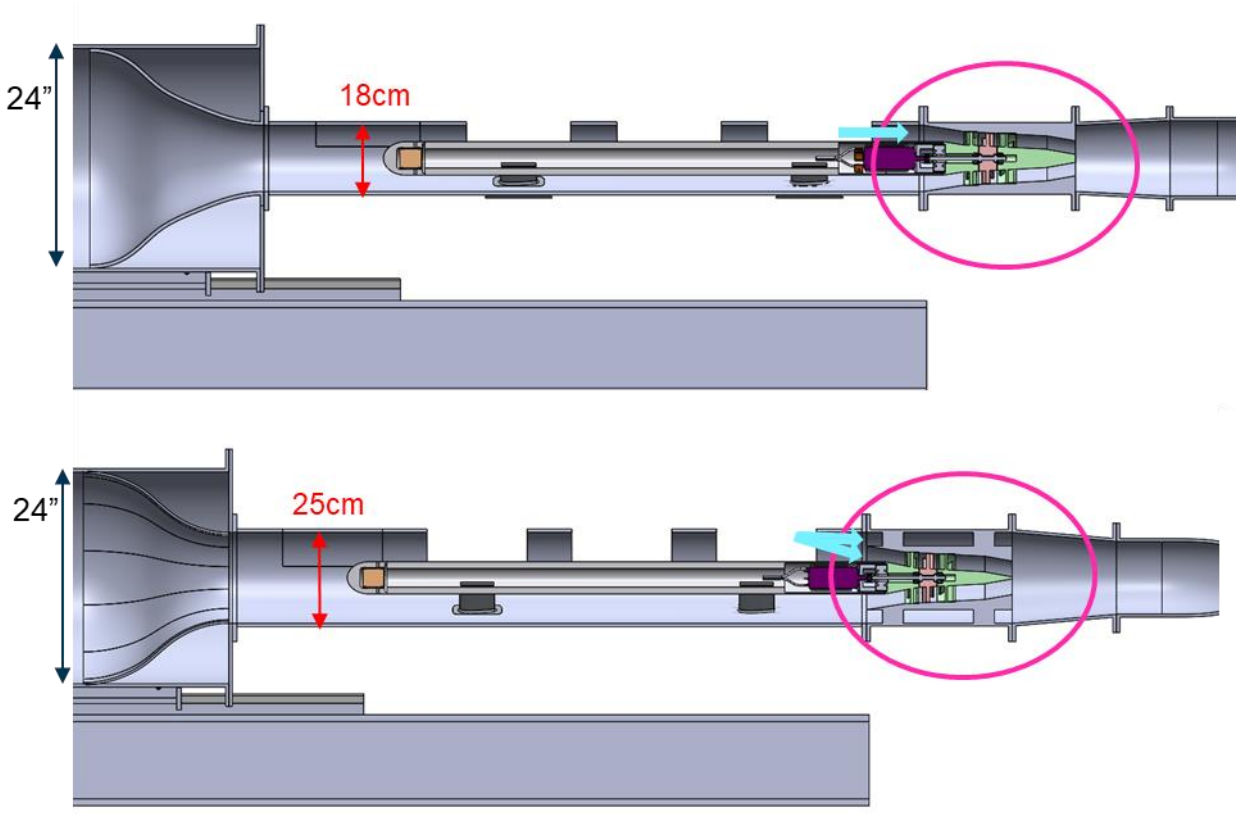

Figure 8 – Preliminary design of the bypass section

To achieve a better flow field, some more modifications were applied such as changing the test unit shape at the bypass nacelle section to be more streamlined. Figure 9 shows the new model and the dimensions that were used for the numerical analysis.

The applied CFD model was steady state and pressure based. The solution method was SIMPLE and the k-epsilon turbulence model with standard wall functions was selected. The boundary conditions included pressure-inlet, mass-flow-outlet, wall, and fan with pressure jump resembling the propulsion system. The entire solution domain was discretized by an unstructured grid and a boundary layer mesh applied adjacent to the walls, Figure 10.

In Figure 11, the velocity vectors at the mid plane of the test rig (y=0), and the velocity profiles at the

fan plane (shown by red line in the pictures) are compared. The purpose was to check how changing the exit mass flow rate can affect the fan mass flow rate and the velocity profiles. The inlet total pressure was set to 24 kPa and the fan pressure rise was 7.2 kPa. The exit mass flow rate was varied between 1.2 to 2.5 kg/s. The velocity vectors results show that the flow is smooth passing through the bypass nacelle except at the exit that due to the sharp trailing edge, where some vorticities are formed. The fan mass flow rate increases by increasing the exit mass flow rate of the test rig, however, its percentage relative to the exit mass flow rate is decreased. It means more flow also passes through the bypass section. The growth of the velocity profiles in bypass section also confirms this.
Additional modifications were applied on the bypass nacelle geometry, as shown in Figure 12. The circular leading and trailing edges were added to the profile. For the upper profile, a constant radius curve tangent to the leading and trailing edges was added, and the lower profile followed the shroud curve. The cross section view of the test rig with the modified bypass nacelle can also be seen in Figure 12.

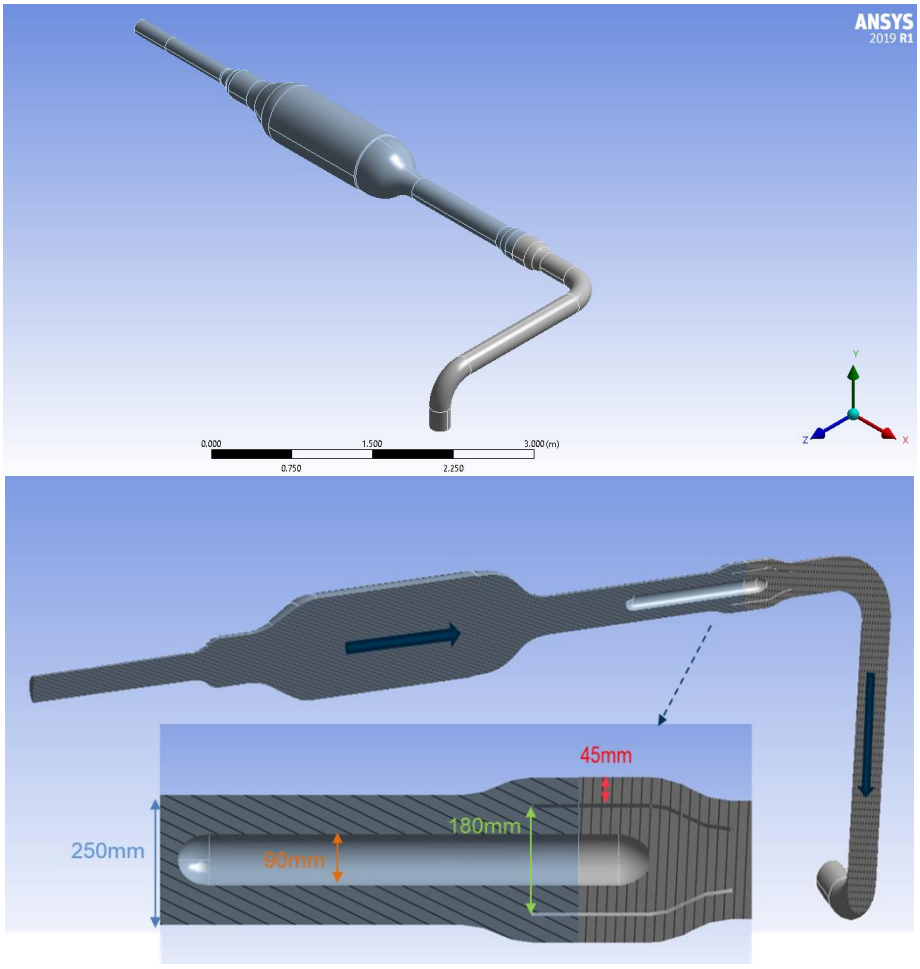

Figure 9 – CFD model for the modified bypass nacelle

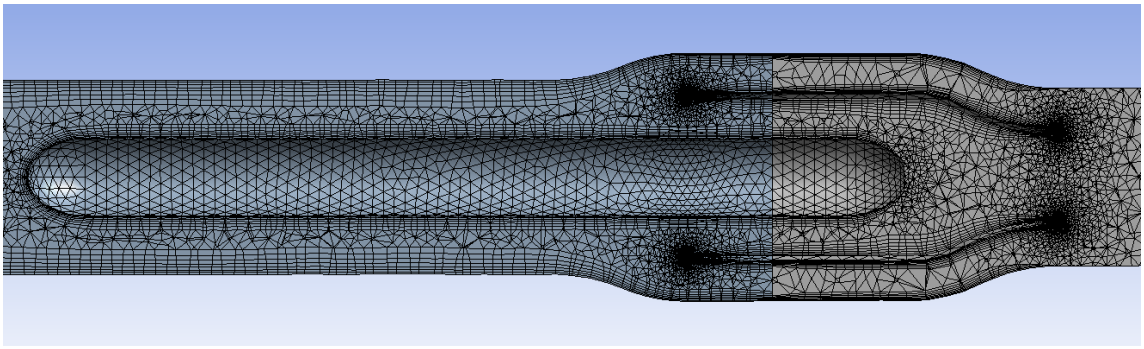

Figure 10 – A view of the mesh for the model with bypass nacelle

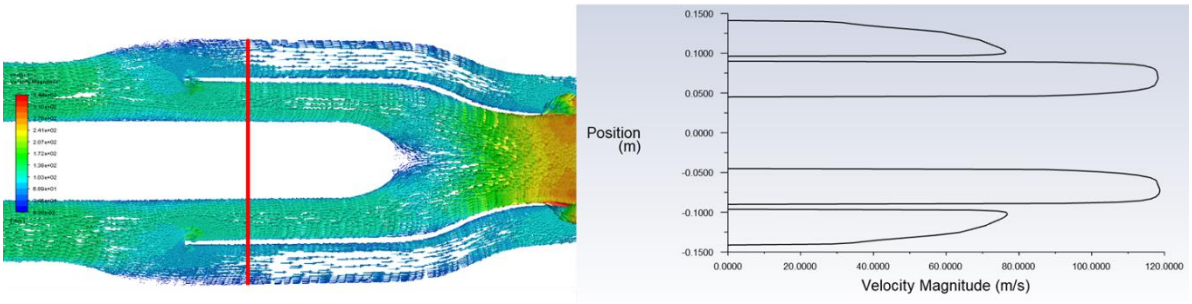

a) $\dot{m}_{exit}$=1.2 kg/s, $\dot{m}_{fan}$=0.62 kg/s= 51%$\dot{m}_{exit}$

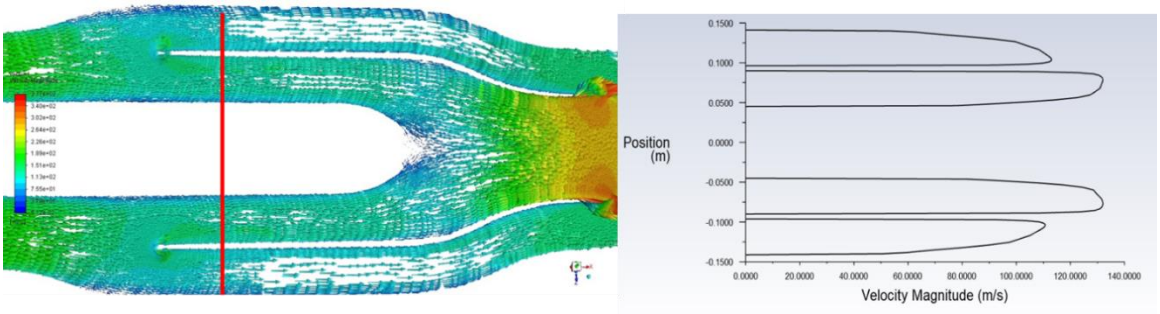

b) $\dot{m}_{exit}$=1.6 kg/s, $\dot{m}_{fan}$=0.68 kg/s= 42%$\dot{m}_{exit}$

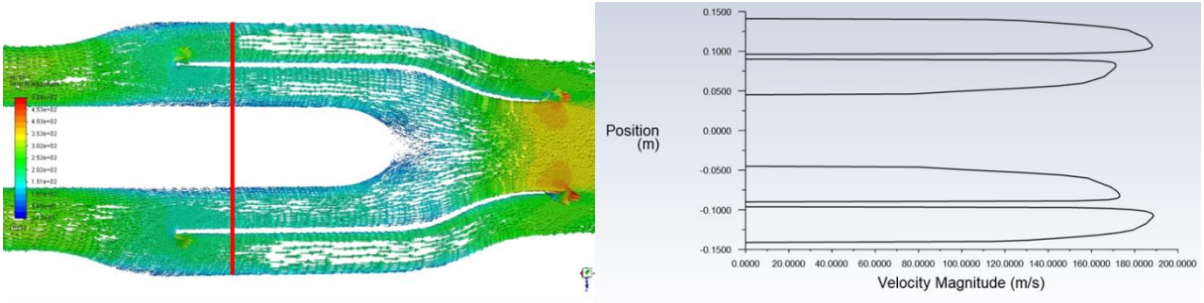

c) $\dot{m}_{exit}$=2.5 kg/s, $\dot{m}_{fan}$=0.85 kg/s= 34%$\dot{m}_{exit}$

Figure 11 – Comparison of velocity vectors and profiles with varying the exit mass flow rate

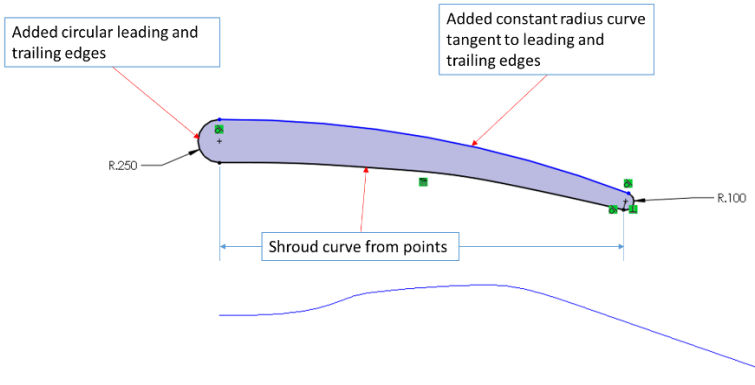

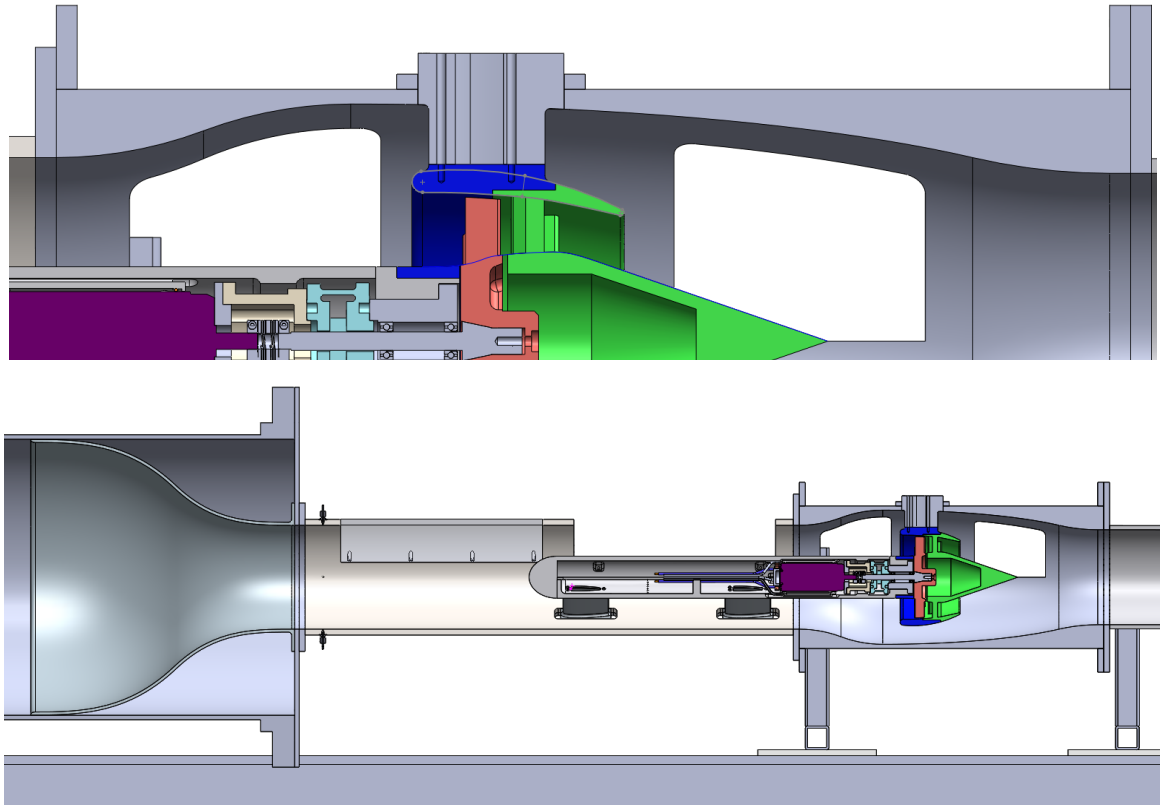

Figure 12 – Bypass nacelle profile modification

3.2 Effect of the Struts

The boundary layer body is supported with three nacelle struts, two forward struts and one aft bottom strut. The electrical power and coolant are provided to the boundary layer body via these hollow struts that have NACA0015 cross sections with different chord sizes. They are positioned to create boundary layer disturbances similar to those seen over a fuselage, such as those due to vertical tail and engine pylon structures.

Figure 13 shows the model used for the numerical simulation. A cross-section of the geometry of the boundary layer body with the struts and the applied meshing are shown in Figure 14. The results including total pressure contour along with the streamlines and velocity vectors are plotted in Figure 15 for inlet total pressure of 24 kPa, fan pressure rise of 7.2 kPa, and exit mass flow rate of 1.5 kg/s. It seems that struts do not disturb the flow and streamlines are smooth everywhere. In this case the resulting mass flow rate of the fan is 0.82 kg/s. Figure 16 shows the non-dimensional total pressure contour at the fan inlet face and the profiles along the radial locations of 12 and 3 o'clock and about 60 degrees which corresponds to the maximum distribution of the total pressure in fan plane. The total pressure is normalized using the average total pressure at the fan face. The effect of vertical tail and engine pylon on the total pressure pattern at the fan face is achieved using the upstream vertical and two forward supporting struts.

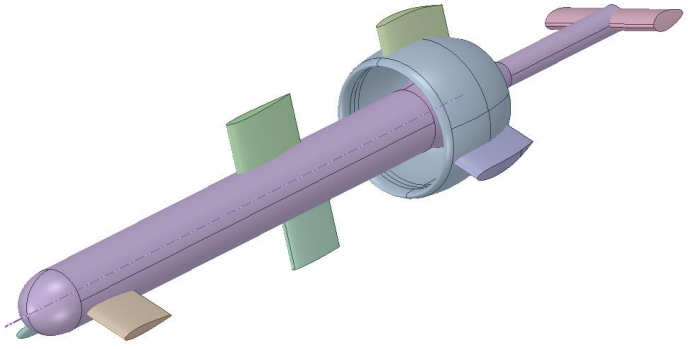

Figure 13 – The boundary layer body model with aft support

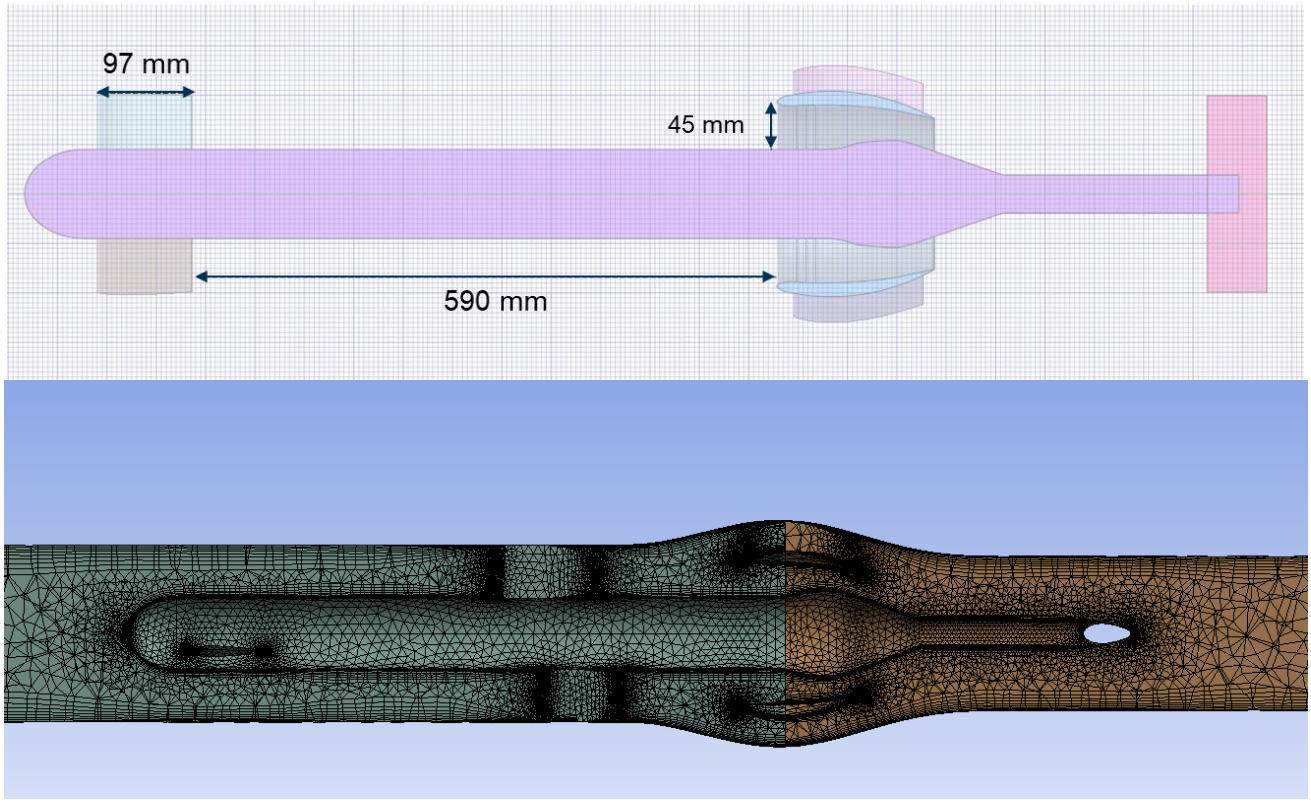

Figure 14 – Geometry and mesh of the boundary layer body with three nacelle struts and aft support

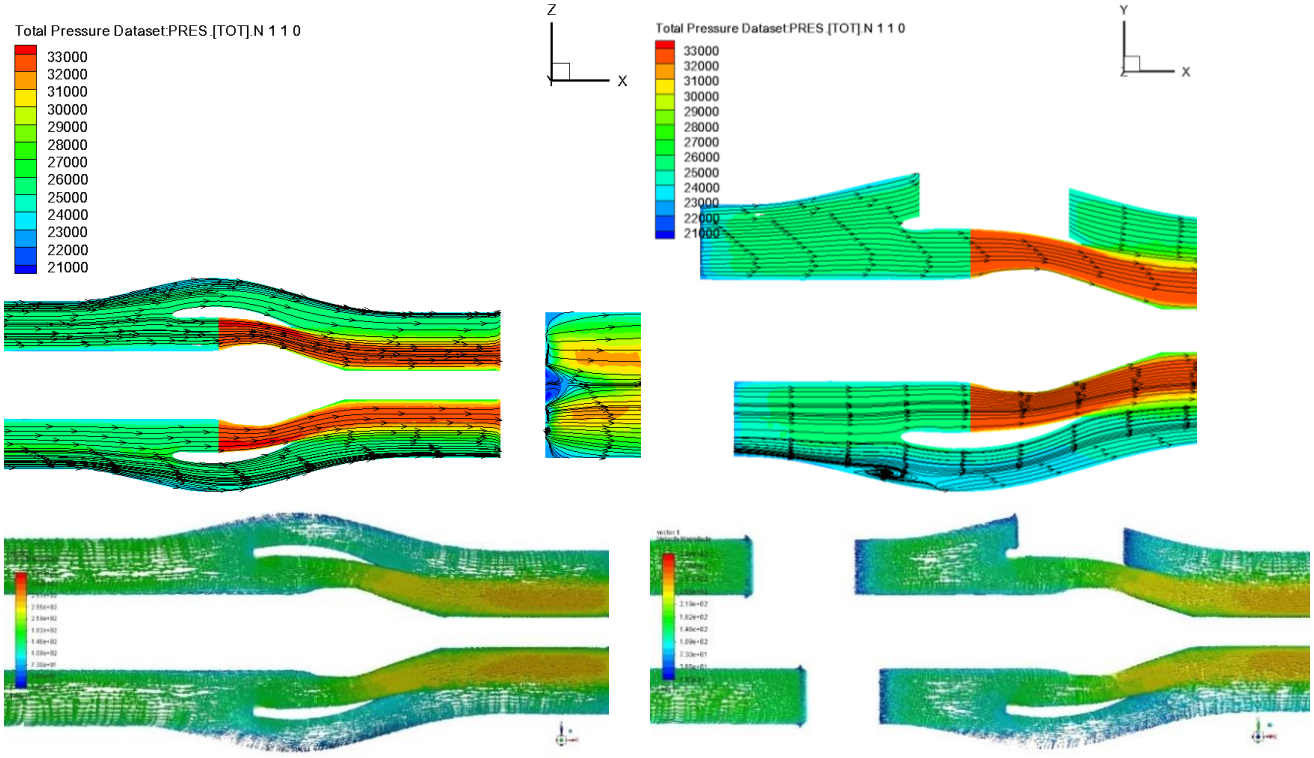

Plane *y*=0 Plane *z*=0

Figure 15 – Streamlines and velocity vectors, P_o=24 kPa, ΔP_{fan}=7.2 kPa, $\dot{m}_{exit}$=1.5 kg/s

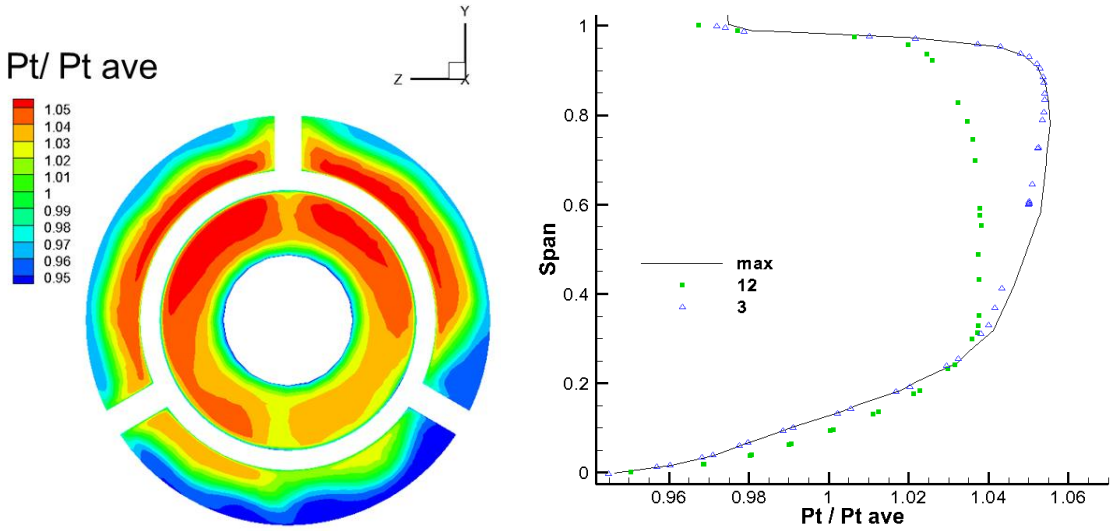

Figure 16 – Non-dimension total pressure distribution at the fan inlet face, P_o=24 kPa, ΔP_{fan}=7.2 kPa, $\dot{m}_{exit}$=1.5 kg/s

3.3 Modification from Three-Strut Configuration into Two-Strut

It was suggested to replace the three struts holding the nacelle by two horizontal struts as sketched in Figure 17. This way, they could be used for side-to-side adjustment and the vertical struts on the boundary layer body could be used for up-down adjustments. However, this would require that all instrumentation wiring such as probes, pressure sensors and speed sensor pass through only two struts.

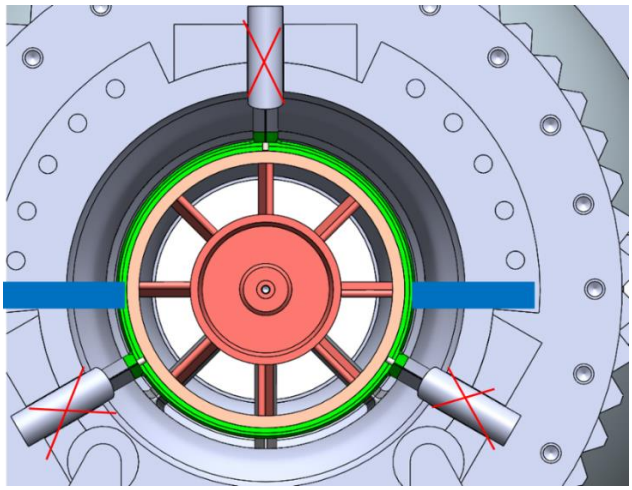

Figure 17 – The two-strut vs. three-strut holding the nacelle

With the new configuration, the CFD analysis was applied. The model with two horizontal struts and the meshing is provided in Figure 18. To decrease the processing time, only the test section part was modeled with the inlet and outlet boundary conditions as shown in Figure 18. The total pressure contours along with the streamlines and the static pressure contours can be seen in Figure 19. It seems the flow is uniform and there is no flow reversal, so the modification was confirmed from an aerodynamics point of view. The resulting mass flow rate of the fan is 0.78 kg/s.

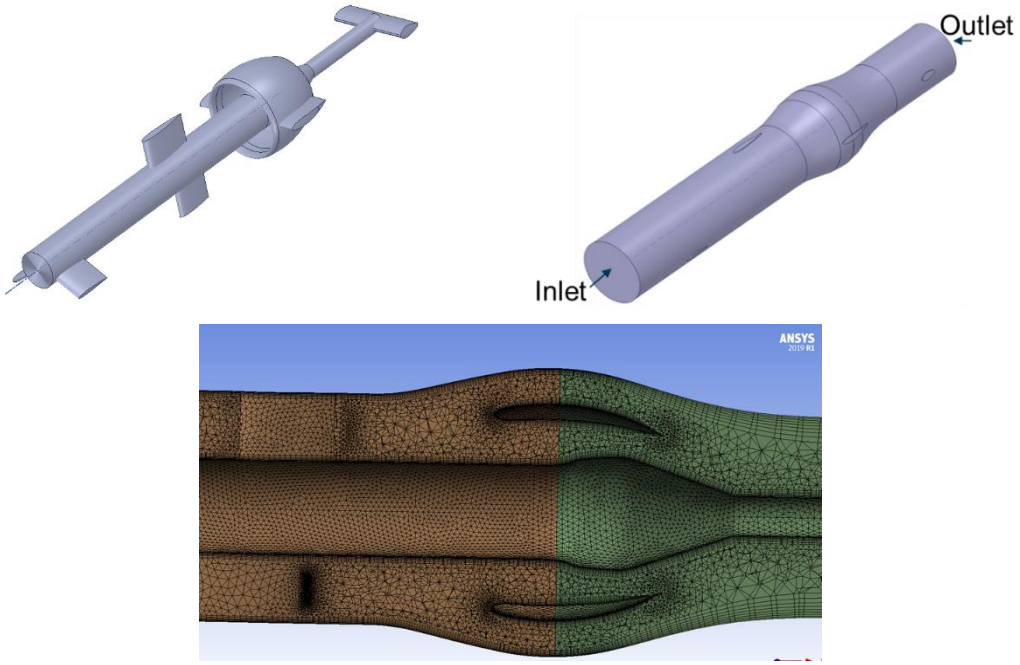

Figure 18 – Modified boundary layer body model for holding the nacelle by two struts

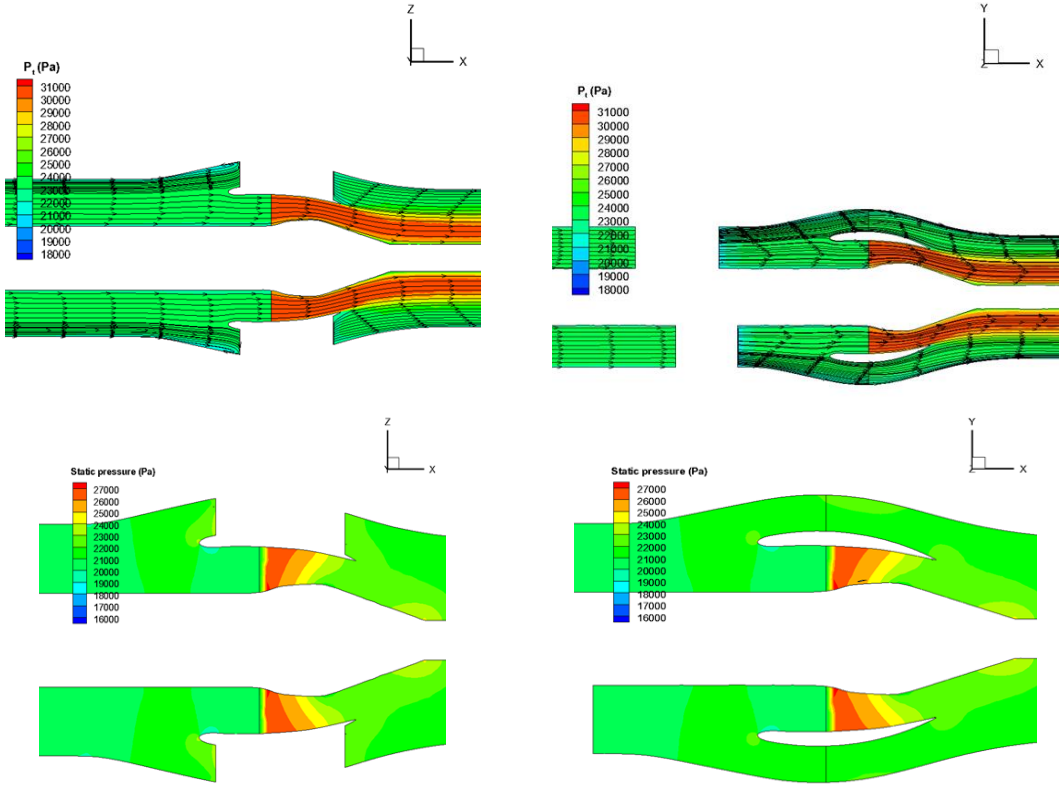

Plane *y*=0 Plane *z*=0

Figure 19 – Streamlines and static pressure contours, P_o=24 kPa, ΔP_{fan}= 6.72 kPa, $\dot{m}_{exit}$=1.3 kg/s

The total pressure and velocity magnitude contours at the fan inlet face are plotted in Figure 20. The corresponding velocity profiles along the radial locations of 12, 6 and 3 o'clock are sketched in Figure 21. The boundary layer thickness is about 40-50% of the span which is 45 mm.

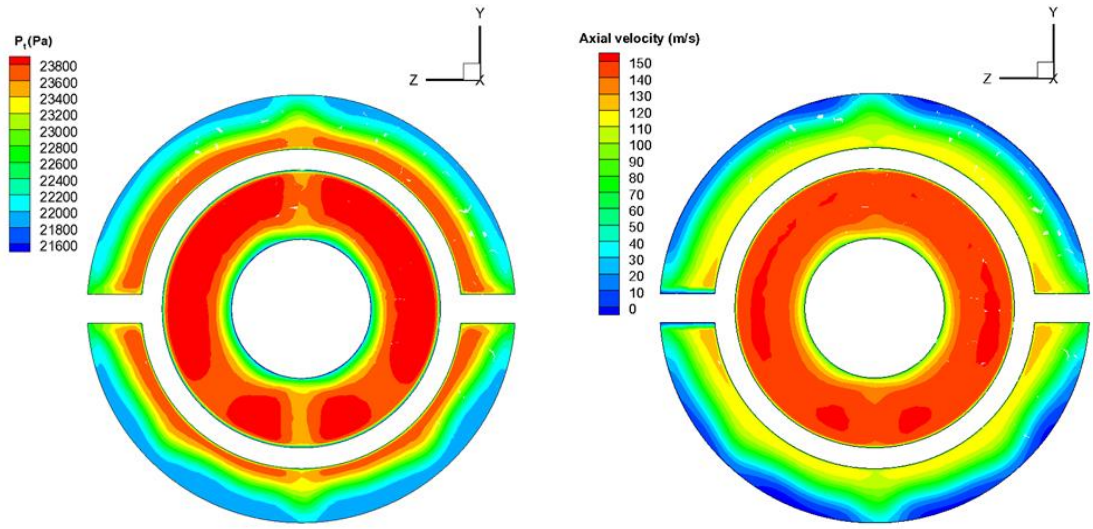

Figure 20 – Total pressure and axial velocity contours at the fan inlet face, P_o=24 kPa, ΔP_{fan}= 6.72 kPa, $\dot{m}_{exit}$=1.3 kg/s

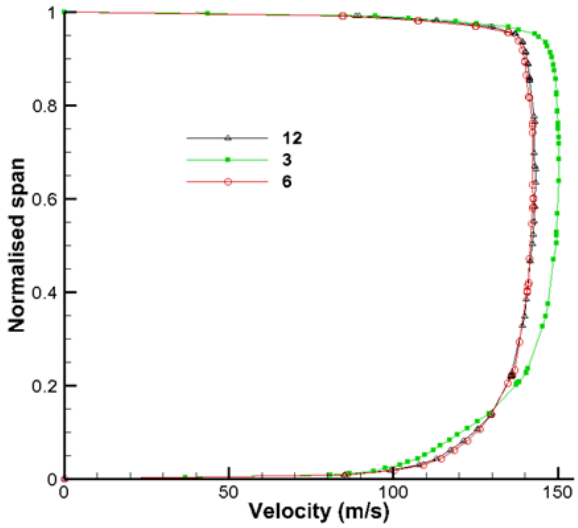

Figure 21 – Velocity profile at the fan inlet face

3.4 Nacelle Strut Modifications

It was required to reinforce and change the size of the nacelle struts because of some changes in measurement instruments passing through them. Analyzing the flow field, it was realized that due to the blunt shape of the trailing edge of the nacelle struts, some flow separation occurs. To avoid it, a modification was applied at the trailing edge to make it sharper, as shown in Figure 22.

The contour of the total pressure along with the stream lines, and the contour of static pressure ratio with respect to the inlet total pressure are plotted for the mid plane of the *z*-direction in Figures 23 to 25. The exit mass flow rates of the rig as well as the fan pressure rise are varied which results in different mass flow rate of the fan and varying the pressure distribution. From Figure 23 and Figure 24, it can be seen that the streamlines are smooth everywhere due to the favorable pressure gradient. The resulting mass flow rates of the fan are 0.78 kg/s and 0.8 kg/s for the conditions of Figure 23 and Figure 24, respectively. However, as shown in Figure 25, with the exit mass flow rate of 1 kg/s, the static pressure downstream of the nacelle increases, so this adverse pressure gradient results in flow reversal in the by-pass section.

Figure 26 shows the variation of pressure ratio and by-pass-ratio with the exit mass flow rate of the rig. For the lowest studied exit mass flow rate (i.e. 1 kg/s), the pressure ratio is very close to one and the by-pass-ratio is very low that confirms the flow reversal in the by-pass section. To resolve this problem, a blockage plate needs to be installed at the fan nozzle to force the flow passing through the by-pass section.

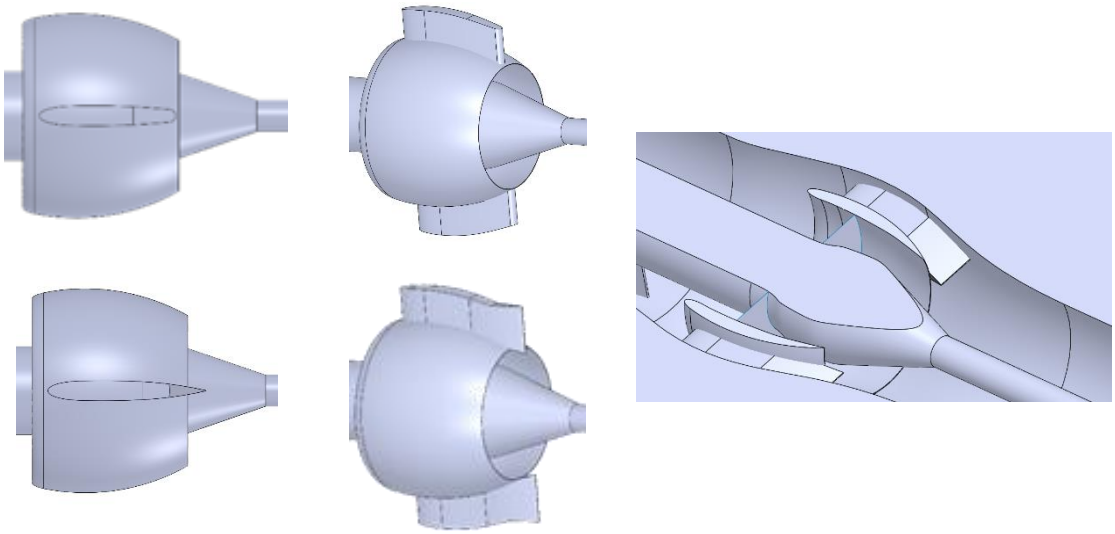

Figure 22 – Additional modifications on nacelle struts due to flow reversal effects

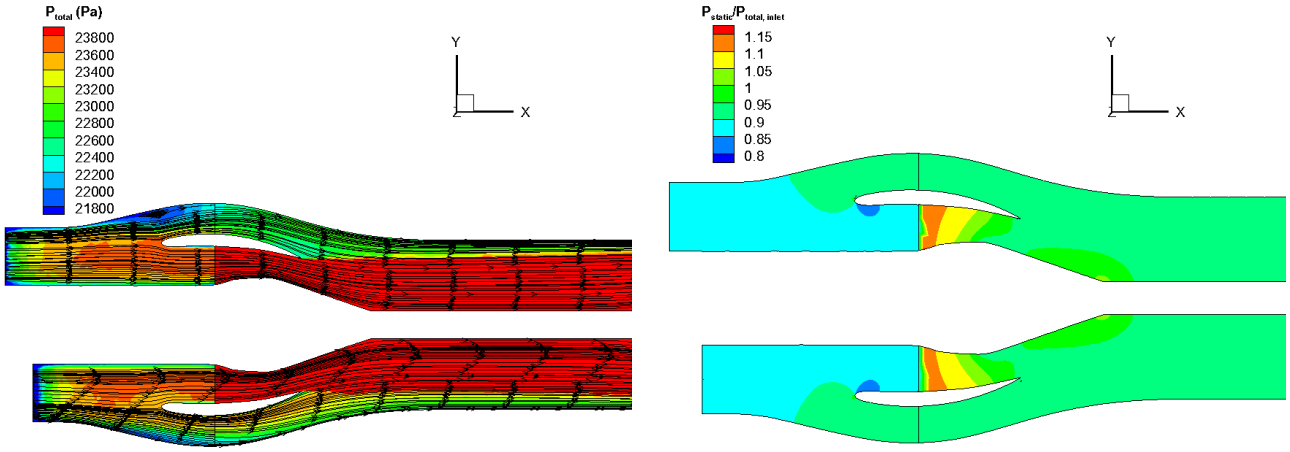

Figure 23 – Total pressure and static pressure ratio contours and streamlines, $\dot{m}_{exit}$=1.3 kg/s ΔP_{fan}=6.72 kPa, plane z=0

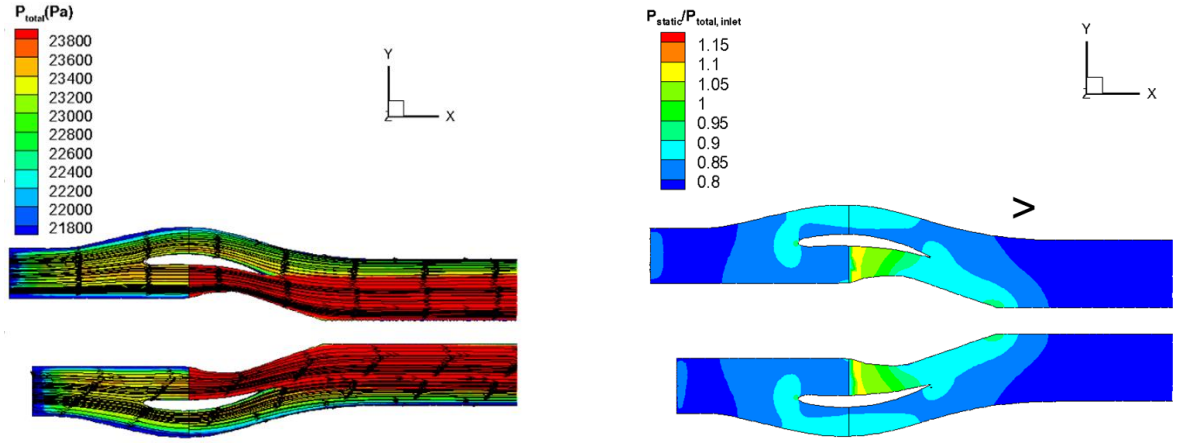

Figure 24 – Total pressure and static pressure ratio contours and streamlines, ΔP_{fan}=5.76 kPa, $\dot{m}_{exit}$=1.7 kg/s, plane z=0

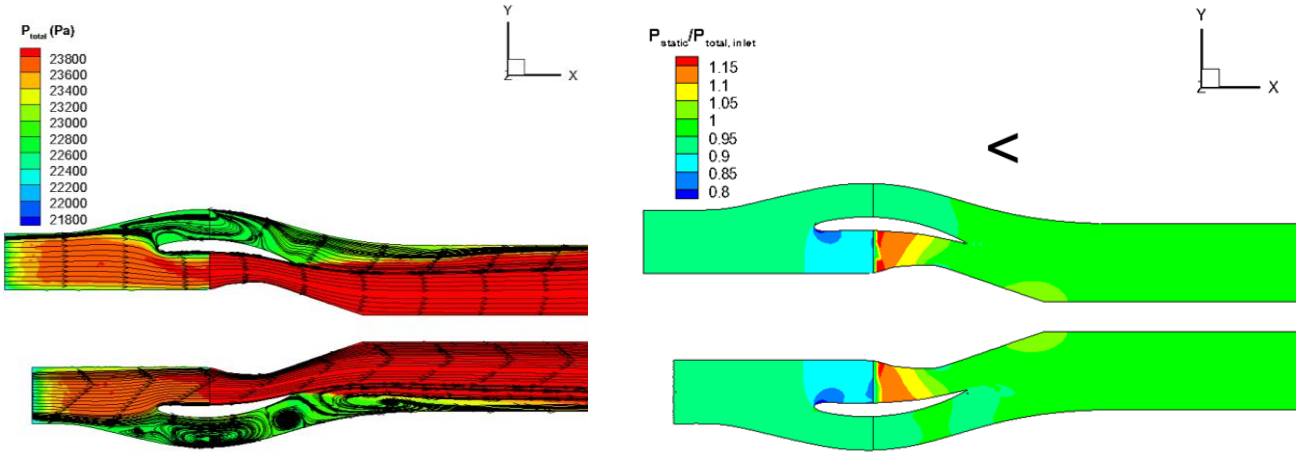

Figure 25 – Total pressure and static pressure ratio contours and streamlines, ΔP_{fan}=7.44 kPa, $\dot{m}_{exit}$=1 kg/s, plane z=0

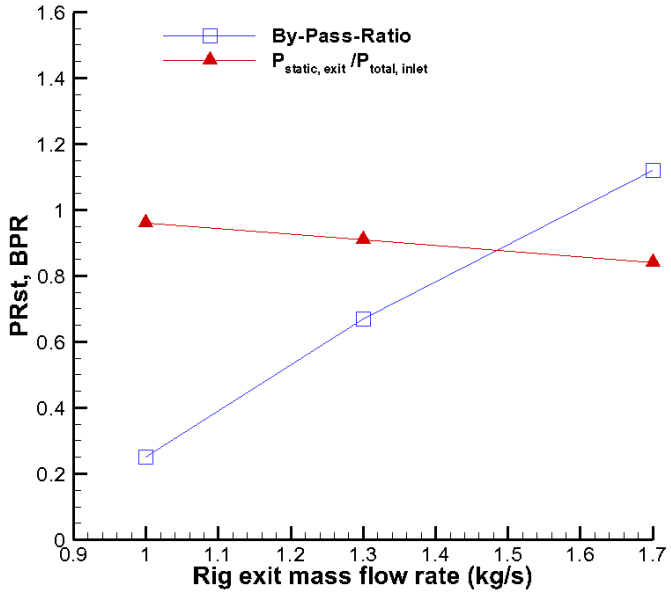

Figure 26 – Variation of pressure ratio and by-pass-ratio

4. Concluding Remarks

Detailed design of the BLI rig capable of achieving representative cruise flight altitudes and Mach numbers was provided. The remaining tasks involve fabrication of the models, facility setup, testing and analysis. This work will serve as a test bed or proof of concept for future full-scale engine BLI studies and understand the technology gaps that need to be overcome to implement this technology into aircraft. Also it gives the capability to do further testing to investigate the effect of ingestion events (e.g. rain, hail, ice ingestion) and different BLI fan designs.

Acknowledgments

The authors would like to acknowledge the contributions of Hugo Breton from the NRC Design and Fabrication Services for his great work and interest in designing the facility.

References

[1] Smith, L.H., Wake ingestion propulsion benefit, *AIAA Journal of Propulsion and Power*, Vol. 9, No. 1, pp. 74-82, 1993.

[2] Tillman, T. G., Hardin, L. W., Moffitt, B. A., Sharma, O. P., Lord, W. K., Berton, J., and Arend, D. System-

level benefits of boundary layer ingesting propulsion, *AIAA 49th Aerospace Sciences Meeting*, 2011.
[3] Liebeck, R. H., Design of the blended wing body subsonic transport, *Journal of Aircraft*, Vol. 41, No.1, pp. 10-25, 2004.
[4] Kawai, R. T., Friedman, D. M., and Serrano, L., Blended wing body (bwb) boundary layer ingestion (BLI) inlet configuration and system studies, NASA/CR-2006-214534, 2006.
[5] Florea, R. V., Matalantis, C., Hardin, L. W., Stucky, M., Shabbir, A., Sharma, O., and Arend, D., Parametric analysis and design for embedded engine inlets, *49th AIAA/SAE/ASEE Joint Propulsion Conference*, AIAA 2012-3994, 2012.
[6] Turnbull, A., Jouan, H., Giannakakis, P., and Iskveren, A. T., Modeling boundary layer ingestion at the conceptual level, *23rd International Society for Air Breathing Engines Conference*, ISABE-2017-22700, 2017.
[7] Sun, D.W., and W. Eames, I., Recent developments in the design theories and applications of ejectors- a review, *Journal of the Institute of Energy*, pp. 65-79, 1995.
[8] Ameur, K., Aidoun, Z., and Ouzzane, M., Modeling and numerical approach for the design and operation of two-phase ejectors, Applied Thermal Engineering, Vol. 109, pp. 809-818, 2016.
[9] Ruangtrakoon, N., Thongtip, T., Aphornratana, S., and Sriveerakul, T., CFD simulation on the effect of primary nozzle geometries for a steam ejector in refrigeration cycle, *International Journal of Thermal Sciences*, http://dx.doi.org/10.1016/j.ijthermalsci.2012.07.009, 2012.
[10] Besagni, G., Mereu, R., Chiesa, P., and Inzoli, F., An Integrated Lumped Parameter-CFD approach for off-design ejector performance evaluation, *Energy Conversion and Management*, Vol. 105, pp. 697- 715, 2015.
[11] Scott, D., Aidoun, Z., Bellache, O., and Ouzzane, M., An experimental investigation of an ejector for validating numerical simulations, *International Journal of Refrigeration*, Vol. 34, pp. 1717- 1723, 2011.
[12] Rao MV., S., and Jagadeesha, G., Aerodynamic design of supersonic ejectors for wind tunnel applications, *National Conference on Wind Tunnel Testing*, India, 2019.
[13] Rudnitski, D.M., Currie, T., MHI 2000 helicopter nacelle icing certification program, NRC, LTR-ST-2134, 1998.
[14] Turyk, P.J., Simple ejector pump analysis, NRC Laboratory Memorandum, LM-ENG-014, 1988.
[15] ESDU 86030 Ejectors and jet pumps. *Design for steam driven flow*, 1986.
[16] Currie, T., Development of a small modular multi-stage axial compressor for ice crystal icing research, *AIAA Aviation Forum*, AIAA-2018-4133, doi:10.2514/6.2018-4133, 2018.
[17] Neuteboom, M., Chalmers, J., and Currie, T., Validation and instrumentation of a small modular multi-stage axial compressor for ice crystal icing research, *SAE International Conference*, USA, 2019-01-1940, doi:10.4271/2019-01-1940, 2019.

Copyright Statement